Science Advances
AAAS

advances.sciencemag.org/cgi/content/full/5/10/eaax1697/DC1

Supplementary Materials for

Past East Asian monsoon evolution controlled by paleogeography, not CO_2

Alex Farnsworth*, Daniel J. Lunt, Stuart A. Robinson, Paul J. Valdes, William H. G. Roberts, Peter D. Clift, Paul Markwick, Tao Su, Neil Wrobel, Fran Bragg, Sarah-Jane Kelland, Richard D. Pancost

*Corresponding author. Email: alex.farnsworth@bristol.ac.uk

Published 30 October 2019, *Sci. Adv.* **5**, eaax1697 (2019)
DOI: 10.1126/sciadv.aax1697

This PDF file includes:

Supplementary Materials

1. Expanded methods

Here we outline the methods associated with (A) the proxy-based reconstructions of monsoon evolution, (B) the model simulations of monsoon evolution, (C) modern observations and (D) evaluation of prescribed paleogeography of the Himalayan-Tibetan Region (hereafter; HTR).

(A) Proxy-based reconstruction of monsoon evolution

Here we provide an overview of the multi-proxy approach used in the study and how both the qualitative and quantitative reconstructions (Fig. 1a) were synthesized. The proxy-data used is a combination of studies from plant flora and fauna (Tables S1 and S2) and other indirect terrestrial and marine proxies used to derive precipitation estimates. An issue with reconstructing monsoon precipitation history in East Asia (EA hereafter) is that the monsoon is highly spatially variable, being wetter, warmer, colder, saltier or windier from one location to the next (*32*), due to local processes associated with, for example, topographic height and steepness. As such, individual proxies should not be taken as indicative of a wider regional signal alone. Therefore, we only present data which is made up of a large number of underlying sites, covering a relatively large area. The use of multi-proxies can alleviate the problem of low spatial and temporal resolution given enough data sites.

(A1) Qualitative records:

Indirect terrestrial and marine proxies have been used to reconstruct the strength of the precipitation (*61*). In isolation, climatically sensitive proxies for precipitation can be controversial and misleading (*5*). However, by using a synthesis of several different proxies and analytical techniques, more robust information can be derived giving greater confidence in the information presented (*5*).

The strength of using indirect paleo-monsoon proxies is that they can infer the trend in monsoon intensity over geologic time periods. For example, the characteristics of a paleosol will give information about the depositional system and paleoclimate. If the record contains evaporitic cements, which decrease in abundance through the record it can be inferred that aridity of the climate lessened because evaporitic minerals are in higher abundance in more arid climates and less abundant in humid climates (*62*). Similarly, pollen assemblages can help classify the paleoenvironmental conditions as, for example, humid versus dry.

For the Cretaceous, we use the lithological record of Hasegawa (*31*). The sites are latitudinally well distributed between 16°N-46°N, giving an indication of the large-scale monsoon system. Figure 1(a) is unmodified from the original but only shows data up to 40°N because north of this latitude is outside the defined modelled monsoon region (fig. S4). In addition, the Tarim Basin was removed from the compilation due to half of the record being missing. The lithological record suggests the environment in which the deposits were formed - in general fluvial, lacustrine, and coal deposits were wetter, whereas red-beds and dunes suggest drier conditions.

For the Paleocene and Eocene, we use the palynological and paleobotanical data of Guo (*4*) and Wang (*34*), which we synthesize in Figure 1a. Much of the data used by Guo (*4*) and Wang (*34*) is contained in Sun and Wang (*6*) but unlike these studies we rotate each individual site back to the Paleocene, Eocene, Oligocene, Miocene and Pliocene locations consistently with our model simulations to gain a more accurate representation of these time periods. The data characterize a large number of sites across EA as representative of ‘humid’ or ‘arid’ environments. From this, we constructed latitudinal banded averages. Threshold criteria to determine the environmental conditions have been devised: where proxy-data within the 5° latitudinal band contains >70% ‘humid’ (‘dry’) conditions it is deemed a ‘humid/sub-humid’ (arid/semi-arid) environment indicative of a strong (weak) monsoon. The

region is classified as ‘semi-arid/sub-humid’ if the proxy-data sites contain <70% ‘humid’ or ‘arid’ regions within the latitudinal band. Classifications are those used in Guo, et al. 2008 (*4*).

Finally, we also incorporate erosional and weathering proxies from Ocean Drilling Program (ODP) Sites 1146 and 1148 (~19°N-16.5°E) in the South China Sea (*32*), spanning from the end of the Oligocene (23 Myr) to the Present-day. We do not include data from the Pliocene or Pleistocene due to the record being strongly influenced by both the local collision in Taiwan and glacial-interglacial transitions, which will have a marked impact of monsoon variability. Here we use the same classification as Clift, et al. 2008 (*5*) (their Fig. 8), describing the system as ‘Monsoonal’, ‘Intermediate’ or ‘Dry’ conditions, with ‘intermediate’ signifying ‘Tropical not monsoonal’, representative of the climate transitioning to a stronger monsoon dominated environment (Fig. 1a; dashed red line).

(A2) Quantitative records

We synthesize the various quantitative proxy records from an extensive compilation of the literature (Tables S1, Supplementary Information) which come from a range of geographical regions across EA, cover different time periods, and do not always overlap in time. As such, creating a coherent precipitation trend over tens of millions of years is problematic; therefore, we normalize the various proxy data as described below. Where mean or best-estimate precipitation values are not given in the literature, the center of the precipitation range is used. The underlying precipitation data are derived from a number of proxies based on the Nearest Living Relative (NLR) (*63, 64*) or Climate-Leaf Analysis Multivariate Program (CLAMP) (*6, 61*) methodologies. There are inherent uncertainties (which represent the minimum uncertainty) in each of these approaches that constrain the specific variables being reconstructed (see table S1). There are, in general, four major components to uncertainties

affecting all of these techniques leading to a predicted range in a reconstructed climatic variable. 1) Taphonomic uncertainty. 2) The statistics of weather used in the calibration uncertainty. 3) Spatial ecosystem heterogeneity uncertainty and 4) sampling uncertainty, which requires a minimum sample size for both calibration and prediction.

Taphonomic uncertainty is generated by a loss of information in the fossilization process, for example a loss of leaf characters used to identify a species and its adaptation to its climate. In practice this source of uncertainty has minimal impact on the overall uncertainty in CLAMP (*65*).

Climatic uncertainty which by in large is a result of the statistics of weather and the variability (diurnal, seasonal, interannual) that can arise within a specified time frame (usually a 30-year mean) for a region in which a particular species inhabits. Most regions are well recorded with observational data spanning many decades, however there are localities (e.g. Africa (*66*) where there are no long-term observations available and gaps in records due to conflict or instrument failure, or changes in recording platforms (*67*).

Spatial ecosystem heterogeneity uncertainty results from the array of species responses to the many different microclimates present in a given region. The full morphological range exhibited by all the species in a heterogeneous ecosystem will produce a climate signal that is dissimilar to that based on just one species inhabiting that ecosystem. Thus, the more species and characteristics preserved within the fossil assemblage the more representative the climate signal will be of the larger scale climate rather than potential microclimates that can exist within the particular ecosystem. For example, plants that inhabit the shady sub canopy where it is cooler and more moist might be expected to have traits that are characteristic of this and different to those of plants that comprise the canopy and are exposed to the free air and

sunnier warmer conditions. In isolation both species would produce a climate signal that is different to one another (*65*).

Sampling uncertainty can arise when strategies are unconstrained and do not adhere to a rule based approach. For example, sampling of a given region where strong gradients in climate can exist (e.g. large topographic gradients, change aspect by measuring different slopes of a mountain) can result is a large predicted climate range, which is a result of a change in elevation rather than a change in climate.

The proxy community is well aware of these uncertainties and has made great strides into constraining them to allow a more robust climate signal to be revealed through geologic time.

The average values (Tables S1) from the various proxies are binned into their appropriate geologic stage (i.e. Albian stage mid-point (~105 Myr); Ext Data Fig. 1e). Only data that spans at least three geologic-stage boundaries are used in the analysis.

The average of the proxy data points (Ext Data Fig. 1a-c) are then scaled between 0 and 1 (Eq. 1; Ext Data Fig. 1d), to form a normalized precipitation for Stage *j*, NP_j

$$NP_j = \frac{\bar{p}_j - 350}{1400 - 350} \qquad (1)$$

Where the mean precipitation (mm/day) in the EA region for stage j, $\bar{p}_j$, is given by

$$\bar{p}_j = \frac{1}{n} \sum_{i=0}^{n} P_i$$

Where P_i (mm/day^{-1}) is the precipitation value from site *i*, from a total of *n* sites for stage *j*. The NP for the various stages then forms the trends in Figure 1a. Note that this quantitative

trend will still be locally biased, and although it represents the average of several locations, it is not directly comparable to the model trend, which represents a true regional average.

(B) Model simulations of monsoon evolution

Here we describe the paleogeographic boundary conditions, climate model, and experimental design used in this study.

(B1) Paleogeographies

The reconstruction of tectonics, structures, and depositional environments that underpin this study were created by Getech Plc. using methods based on those of Markwick and Valdes (*63*). The paleo-digital elevation models used as boundary conditions in the model for each stage are informed by these reconstructions, which are in turn constrained by extensive geological databases. These data include published lithologic, tectonic and fossil studies, the lithologic databases of the Paleogeographic Atlas Project (University of Chicago), and deep sea (Deep Sea Drilling Project (DSDP)/ODP) data, as well as data such as from the Atlas projects databases (*64*). They are extensively updated from the series described in Markwick (*68*); they include bathymetric information for running coupled atmosphere-ocean climate models. These data are also used to develop the plate model on which the paleogeographies are built. The paleogeographies were produced at an original resolution of 0.5° × 0.5°, and from these we generated model-resolution (3.75° × 2.5°) land-sea mask, topography and bathymetry, and the sub-gridscale orographic variables required by the model. These model-resolution paleogeographies are shown here in fig. S1. These reconstructions mainly represent the maximum transgression of sea level for the time-slices. Higher transgression shorelines will result in warmer and wetter worlds to a degree as the larger ocean surface is not only a large moisture source but also a greater energy store (*63*) owing to oceans have a

higher heat capacity in comparison to land. For more details, see Lunt, et al. 2016 (*60*). Evaluation of the prescribed paleogeographies is given in Section (D) of this supplement.

For a robust comparison of model precipitation versus the proxy record we consistently rotate the modern-day monsoon region back through time with the paleogeographies. This allows accurate comparison of model precipitation with the location of the proxy site for each geologic stage simulated.

In addition, we carry out six simulations (stages: Valanginian, Albian, Turonian, Maastrichtian, Chattian and Paicenzian) with paleogeographies produced independently from, but using similar methods to, the Getech paleogeographies. These are illustrated in Supplementary Information fig. S8. Roberstons Plc provides these reconstructions, following a similar methodology to that described for the Getech Plc Reconstructions, also including exploration data that is not in the public domain to further constrain the reconstructions. The key aspect here is that the uncertainty in the paleogeography of a single Stage (expressed as the difference between the Robertsons and Getech paleogeographies) is in general less than the difference in paleogeography between different Stages.

(B2) Model description and modern evaluation

The HadCM3L General Circulation Model (GCM) version 4.5 (3.75° x 2.5° longitude x latitude atmosphere and ocean resolution), which is a low resolution version of HadCM3 (*69*) (3.75° x 2.5° atmosphere resolution, 1.25° x 1.25° ocean resolution) version, is used for these model simulations. HadCM3L consists of 19 vertical levels in the atmosphere and 20 vertical levels in the ocean using the Arakawa B-grid scheme. HadCM3L solves the fundamental equations of fluid dynamics on a rotating sphere, and represents thermodynamic and radiative transfer of heat at a grid scale. Sub-grid scale processes such as those associated with clouds are parameterized as they cannot be explicitly resolved. Flux adjustments (artificial heat and

salinity adjustments in the ocean to prevent the model drifting to unrealistic values) are not required in this model (*70*), which is highly desirable for long paleoclimate simulations.

Parameterizations include the radiation scheme of Edwards and Slingo (*71*), the convection scheme of Gregory (*72*), and the MOSES-2.1 land-surface scheme, whose representation of evaporation includes the dependence of stomatal resistance on temperature, vapor pressure and CO_2 concentration (*73*). The ocean model uses the Gent and McWilliams (*74*) mixing scheme. There is no explicit horizontal tracer diffusion in the model. The sea ice model uses a simple thermodynamic scheme and contains parameterizations of ice concentration (*75*) and ice drift and leads (*76*).

TRIFFID (Top-Down Representation of Interactive Foliage and Flora Including Dynamics) the dynamic vegetation model (*73*) was utilized allowing fully coupled two way land-atmosphere interactions. The land surface scheme, MOSES 2.1, was employed, as opposed to MOSES 2.2, due to the former producing a better representation of pre-industrial climates in combination with the TRIFFID model (*77*). TRIFFID allows full interaction between climate and feedbacks associated with vegetation cover and complex land surface-atmosphere interactions, crucial for modelling monsoon systems through geologic time (*78*).

The specific model we use here is "HadCM3LB-M2.1" as described in Valdes (*79*) HadCM3L has not been previously validated against in-situ modern observational measurements with respect to EA monsoon characteristics. However, the model is part of the HadCM3 family which has seen extensive use and contributed to the 3rd to 5th assessment reports of the IPCC (AR3-5). HadCM3 shows good skill in simulating a mean climate state in good agreement with observations in both surface temperature, precipitation, 850 mb winds and mean sea level pressure seasonally and annually in both spatial and temporal distributions in EA (*37, 38*) giving confidence in the basic thermodynamic and hydrologic state. Crucially, HadCM3 also shows skill (*28*) in determining the spatial extent of the

monsoon important for the determination for monsoon evolution and comparison with proxy data. It was found by Jiang (*37*) that HadCM3 performs better in the EA region relative to many other contemporary coupled climate models, and even performs better than the multi-model mean. When the regional average precipitation in EA was compared against modern in-situ observations (CRU) for JJA, HadCM3 produced values of 3.95 mm/day^{-1} compared with 3.94 mm/day^{-1} in the observations (*37*). However, there is a small positive bias in the HadCM3L (pre-industrial simulation) model in annual precipitation compared to CMAP observations in the monsoon region (4.3 mm/day^{-1} and 3.7 mm/day^{-1} respectively). Comparison of the pre-industrial simulation against 1901–1930 Global Precipitation Climatology Centre (GPCC) rain gauge analysis product (*80*), confirms this positive bias (~0.3-0.5mm/day^{-1}) on an annualized and seasonal (Jun-Aug) basis, but is not spatially uniform. We note that teleconnections are important in the response of the EAM, specifically those related to ENSO, and that HadCM3 produces a realistic representation of ENSO characteristics (including the impact of the Asian monsoon system), such as the amplitude, period, and phase locking with the seasonal cycle (*81*). SST proxy comparisons are not evaluated here due to their strong relationship to thermal forcing in response to variable CO_2 concentrations, which are highly uncertain. Although HadCM3L is more seasonal at high latitudes than suggested by the geological record, it does a reasonable job at reproducing the observed seasonality in the modern when compared to ERA-40 reanalysis data (*82*).

(B3) Model Experimental Design:

The simulations described in this paper, except for those of the Neogene, and the CO_2 and paleogeography sensitivity studies, are described in detail, including their experimental design, in Lunt (*60*) Here follows a brief summary of the key points of the experimental design and model initiation and spin-up.

When modelling mean climate states for multi-million-year long intervals it is appropriate to choose a single orbital/astronomical boundary condition for all simulations. For consistency, all simulations use a modern day orbital configuration, which has relatively low eccentricity and an average obliquity compared with average values over the last million years. Solar luminosity for each mid-point geologic stage is calculated according to Gough (*83*). Ice sheets are prescribed with ice sheet extent and volume based on geologic evidence. Although the solar constant varies through the simulations, it changes very slowly and we assume its effects are negligible in terms of the long-term evolution of the East Asian monsoon. When discussing paleogeographic change, for the purposes of this paper we consider the changing ice sheets to be a component of the changing paleogeography. We spin up the model in 4 phases (See Lunt, et al. 2016 (*60*) for details). Changes in boundary conditions during the spin-up leads to the discontinuities in SSTs seen in fig. S5a.

The paleogeographic sensitivity studies are carried out at various CO_2 concentrations, and integrated for varying lengths of time, although all are run for more than 8000 years, and all simulations have reached a steady state.

pCO_2 concentrations are increasingly uncertain further back through the geologic record. *p*CO_2 concentrations back to ~800,000 years ago are well constrained through direct measurement of ice core records (*84*). Beyond the last ~1 million years no direct measurement of atmospheric *p*CO_2 can be obtained, leading to a reliance on indirect indicators. Here we prescribe *p*CO_2 concentrations that are broadly consistent with the record of Foster et al (*3*) but which are primarily intended to be idealized and to allow determination of the role of paleogeography. As such, we choose to prescribe an idealized *p*CO_2 evolution, taking the very broadest features of the *p*CO_2 record into account, but, by prescribing constant CO_2 values over as long a period as possible, this allows us to isolate the solar luminosity and paleogeographic control on monsoon evolution. To further ascertain the

sensitivity of the monsoon system to pCO_2, a series of 15 sensitivity studies were carried out (detailed in Fig. 1c). The pCO_2 sensitivity simulations follow the same methodology as the other simulations. However, in the last one thousand years of the simulation, the pCO_2 concentration was modified (either to 2x 3x or 4x Pre-Industrial concentration) to allow the simulation to approach equilibrium. The prescribed pCO_2 for all the simulations is shown in Figure 1c.

(C) Modern observations:

The CPC Merged Analysis of Precipitation (CMAP) observational dataset is used for comparison against the modern-day model simulation precipitation signal as a validation of the model (see Fig. 1b in the main paper, yellow triangle). CMAP consists of precipitation values derived from five different satellite estimates (GPI, OPI, SSM/I scattering, SSM/I emission and MSU) and rain gauge observations (*39*). Annual precipitation is calculated for the East Asian Monsoon (EAM) region as previously defined in the simulation for accurate comparison. Globally, CMAP precipitation estimations are accurate to within 5–10%, however regional scale estimates can suffer from uncertainties due to the quality and amount of the input data producing varying rainfall estimates (*85*). CMAP has a spatial resolution of 2.5° x 2.5°.

(D) Evaluation of prescribed paleogeography of the HTR:

The modern EAM system is known to be both dynamically and thermodynamically coupled to the HTR region (*86*). Evaluation of the topographical reconstruction used in these simulations against available paleoaltimetry proxy-reconstructions is essential to ensure that the climate signal from the model is consistent with current understanding of the uplift and evolution of the topography in the region.

A comparison of paleoaltimetry data spanning the last 150 Myr with our prescribed paleogeographies at the local (at the grid-point) and regional (all eight grid-points surrounding and including the local grid-point) is given in Tables S3. The paleo-rotated model elevations are within the range estimates of the proxy paleoaltimetry data at a local and regional scale for 50% and 80% of sites respectively. This is perhaps unsurprising given that similar (but greatly expanded by proprietary industry data) paleoaltimtery data was used to generate the prescribed paleogeographies. Figure S2a shows the point-by-point comparison between the median proxy elevation reconstructions in Tables S3 against our climate model paleogeographies. Vertical error bars represent the uncertainty in the proxy reconstruction and lateral error bars represent the age-related uncertainty in the reconstructions as a function of the model elevations (e.g. the grid-point elevation will have a range comprising two or more model elevations if the proxy age constraint is greater than one geologic stage). The prescribed topography shows a similar range of values and slope as the proxy data. In order to verify that our paleogeogeaphies are 'skillful', we make a similar comparison, but instead of comparing the paleoaltimtery data with the prescribed topography from the same time period, we compare with a fixed modern elevation. We find that our prescribed paleo-elevations, although idealized have skill, because a greatly reduced number of points are consistent with the palaeoaltimetry data in the fixed cases – 37% locally and 67% regionally (Tables 3; fig. S2b). However there is still allot of uncertainty in reconstruction as shown by Botsyun, et al. 2019 (*55*) who have recently suggested that the Tibetan Plateau was substantially lower than 3000m in the Eocene using an isotope enabled GCM which is substantially lower than proxy based estimates of >4000m (Table S2).

Code availability:

The UK Meteorological Office made available the source code of HadCM3 via the Ported Unified Model release (http://www.metoffice.gov.uk/research/collaboration/um-partnership) The main repository for the Met Office Unified Model (UM) at the version corresponding to the model presented here can5 be found at http://cms.ncas.ac.uk/code_browsers/UM4.5/UMbrowser/index.html. Further information can also be found in Valdes (2017).

Data availability:

Datasets generated for this paper can be accessed from the University of Bristol BRIDGE research group website: https://www.paleo.bristol.ac.uk/ummodel/scripts/papers/
Images of the boundary conditions are shown in Supplementary information, fig. S1 and S8 and a digital form of the Getech Ypresian simulation is available from Supplementary information in Lunt (2016). The digital Getech paleogeographies for non-Ypresian stages are available from Getech Plc but restrictions apply to the availability of these data, which were used under license for the current study, and so are not publicly available. Data are however available from the authors upon reasonable request and with permission of Getech Plc.
Raw data used to produce figures 1, 2 and 3 as well as figs. S1, S3, S4, S5, S6, S7 and S8 can also be found at this link. Supplementary figure 1 and 3 data can be accessed in Supplementary information; table 1 and 2.

Table S1. Proxy precipitation data in the East Asia Monsoon (EAM) region compiled from various papers (Column 1 and 2), the analysis methodology performed (column 3), modern latitude and longitude of the data site (Column 4 and 5), Age (Ma) the sites have been pale-orotated back to for comparison in the model (column 6), derived mean precipitation from the

associated proxy (column 7), Maximum and minimum range of the derived precipitation (Column 8 and 9) and whether the proxy has been used within Fig. 1a trend (black line). Precipitation proxy-data for each study investigated with the specific site the data is from in these studies given. The type of analysis technique used is also highlighted here (CA - Coexistence Approach, NLR – Nearest Living Relative, ODA – Overlapping Distribution Analysis and CLAMP - Climate Leaf Analysis Multivariate Program). The stage date is also shown (determined by the proxy falls within the individual stage timeframes). Precipitation range is given for the maximum and minimum estimate and the mean of the range. Where the specific dataset has been (*87*) used to calculate the quantitative data trend (Fig. 1a) a 'Y' is denoted.

Author & Date	Site	Analysis	Modern Latitude	Modern Longitude	Age (Ma)	Precipitation (mm/yr)	Max Range	Min Range	In Trend (Fig.1a)
Quan et al., 2012 (*36*)	8	CA	39.9	119.6	44.5	1210	1298	1122	N
Quan et al., 2012 (*36*)	8	CA	39.9	119.6	37.2	1210	1298	1122	N
Quan et al., 2012 (*36*)	9	CA	38.3	117.3	52.2	1210	1298	1122	N
Quan et al., 2012 (*36*)	9	CA	38.3	117.3	44.5	1164	1206	1122	N
Quan et al., 2012 (*36*)	10	CA	36.7	118.8	52.2	907.5	1143	672	N
Quan et al., 2012 (*36*)	11	CA	32.8	119.4	52.2	1194.5	1206	1183	Y
Quan et al., 2012 (*36*)	11	CA	32.8	119.4	44.5	1164	1206	1122	Y
Quan et al., 2012 (*36*)	11	CA	32.8	119.4	37.2	1210	1298	1122	Y
Quan et al., 2012 (*36*)	12	CA	31.9	117.2	52.2	1210	1298	1122	Y
Quan et al., 2012 (*36*)	12	CA	31.9	117.2	44.5	1164	1206	1122	Y
Quan et al., 2012 (*36*)	12	CA	31.9	117.2	37.2	970.5	1206	735	Y
Quan et al., 2012 (*36*)	13	CA	30.9	118.7	44.5	1210	1298	1122	N
Quan et al., 2012 (*36*)	14	CA	27.9	116.1	52.2	1136.5	1151	1122	Y
Quan et al., 2012 (*36*)	14	CA	27.9	116.1	44.5	1240.5	1298	1183	Y
Quan et al., 2012 (*36*)	14	CA	27.9	116.1	37.2	1240.5	1298	1183	Y
Quan et al., 2012 (*36*)	16	CA	22.6	113.3	52.2	1238.5	1355	1122	N
Quan et al., 2012 (*36*)	16	CA	22.6	113.3	44.5	1045	1355	735	N
Quan et al., 2012 (*36*)	17	CA	21.5	110.8	37.2	1321	1520	1122	N
Quan et al., 2012 (*36*)	18	CA	21.1	109.7	44.5	1398	1613	1183	N
Quan et al., 2012 (*36*)	18	CA	21.1	109.7	37.2	1321	1520	1122	N
Quan et al., 2012 (*36*)	19	CA	19.7	110.4	44.5	1357	1520	1194	N
Quan et al., 2012 (*36*)	20	CA	22.1	107.1	37.2	1271	1355	1187	N
Quan et al., 2012 (*36*)	21	CA	23.9	106.6	37.2	1194.5	1206	1183	N
Quan et al., 2012 (*36*)	22	CA	30.4	112.8	52.2	1095.5	1294	897	N
Quan et al., 2012 (*36*)	23	CA	33.8	111.6	52.2	1097.5	1298	897	N
Quan et al., 2012 (*36*)	23	CA	33.8	111.6	44.5	1197	1298	1096	N
Quan et al., 2012 (*36*)	24	CA	34.5	110.8	52.2	1210	1298	1122	N
Quan et al., 2012 (*36*)	25	CA	39.1	107.9	52.2	1210	1298	1122	N
Quan et al., 2012 (*36*)	25	CA	39.1	107.9	44.5	1097.5	1298	897	N
Quan et al., 2012 (*36*)	26	CA	36.1	103.8	52.2	1164	1206	1122	Y
Quan et al., 2012 (*36*)	26	CA	36.1	103.8	44.5	970.5	1206	735	Y
Quan et al., 2012 (*36*)	26	CA	36.1	103.8	37.2	1321	1520	1122	Y
Quan et al., 2012 (*36*)	27	CA	36.2	103.5	37.2	754.5	774	735	N
Quan et al., 2012 (*36*)	28	CA	36.5	101.7	52.2	1126	1355	897	Y
Quan et al., 2012 (*36*)	28	CA	36.5	101.7	44.5	1126	1355	897	Y
Quan et al., 2012 (*36*)	28	CA	36.5	101.7	37.2	1097.5	1298	897	Y
Quan et al., 2012 (*36*)	29	CA	29.9	100.3	37.2	975	1215	735	N
Quan et al., 2012 (*36*)	30	CA	33.1	98.6	44.5	1256.5	1298	1215	N

Quan et al., 2012 (*36*)	31	CA	40.3	97.1	44.5	754.5	774	735	N
Quan et al., 2012 (*36*)	31	CA	40.3	97.1	37.2	754.5	774	735	N
Quan et al., 2012 (*36*)	32	CA	38.3	90.7	44.5	1197	1298	1096	N
Quan et al., 2012 (*36*)	32	CA	38.3	90.7	37.2	1097.5	1298	897	N
Quan et al., 2012 (*36*)	33	CA	35.3	92.3	44.5	1225.5	1355	1096	N
Quan et al., 2012 (*36*)	33	CA	35.3	92.3	37.2	1121	1355	887	N
Quan et al., 2012 (*36*)	34	CA	33.5	90.7	44.5	1238.5	1355	1122	N
Quan et al., 2012 (*36*)	35	CA	29.3	88.9	37.2	1269	1355	1183	N
Quan et al., 2012 (*36*)	36	CA	38.3	77.3	52.2	1227.5	1632	823	Y
Quan et al., 2012 (*36*)	36	CA	38.3	77.3	44.5	1097.5	1298	897	Y
Quan et al., 2012 (*36*)	36	CA	38.3	77.3	37.2	1121	1355	887	Y
Quan et al., 2012 (*36*)	37	CA	41.7	82.9	37.2	1097.5	1298	897	N
Wang et al., 2013 (*34*)	1	CA	31.86	117.28	52.2	1091.65	1389.3	794.05	N
Wang et al., 2013 (*34*)	1	CA	31.86	117.28	44.5	1087.05	1389.4	784.7	N
Wang et al., 2013 (*34*)	2	CA	30.92	118.3	52.2	1102.6	1389.4	815.8	N
Wang et al., 2013 (*34*)	2	CA	30.92	118.3	44.5	1082.5	1389.4	775.6	N
Wang et al., 2013 (*34*)	3	CA	32.6	119	52.2	1102.6	1389.4	815.8	Y
Wang et al., 2013 (*34*)	3	CA	32.6	119	44.5	1071.5	1484.3	658.7	Y
Wang et al., 2013 (*34*)	3	CA	32.6	119	37.2	1021.7	1389.4	654	Y
Wang et al., 2013 (34)	4	CA	31.33	118.38	52.2	1091.65	1389.4	793.9	N
Wang et al., 2013 (34)	5	CA	30.95	118.74	44.5	1091.65	1389.4	793.9	N
Wang et al., 2013 (34)	5	CA	30.95	118.74	37.2	1091.65	1389.4	793.9	N
Wang et al., 2013 (34)	8	CA	36.4	116	44.5	1012.15	1031.3	993	N
Wang et al., 2013 (34)	8	CA	36.4	116	37.2	1012.15	1031.3	993	N
Wang et al., 2013 (34)	10	CA	23	113.26	52.2	1102.6	1389.4	815.8	N
Wang et al., 2013 (34)	10	CA	23	113.26	44.5	1102.6	1389.4	815.8	N
Wang et al., 2013 (34)	11	CA	23.33	113	44.5	1102.6	1389.4	815.8	N
Wang et al., 2013 (34)	11	CA	23.33	113	37.2	1102.6	1389.4	815.8	N
Wang et al., 2013 (34)	12	CA	23.7	107	37.2	1091.65	1389.4	793.9	N
Wang et al., 2013 (34)	13	CA	22.2	107.5	37.2	1560.25	1636.2	1484.3	N
Wang et al., 2013 (34)	14	CA	33.8	111.62	52.2	1130.6	1389.4	871.8	N
Wang et al., 2013 (34)	18	CA	32.5	120	52.2	1102.6	1389.4	815.8	Y
Wang et al., 2013 (34)	18	CA	32.5	120	44.5	1191.2	1389.4	993	Y
Wang et al., 2013 (34)	18	CA	32.5	120	37.2	1191.2	1389.4	993	Y
Wang et al., 2013 (34)	19	CA	25.4	114.34	52.2	1102.45	1389.4	815.5	N
Wang et al., 2013 (34)	20	CA	28	115	44.5	1102.6	1389.4	815.8	N
Wang et al., 2013 (34)	20	CA	28	115	37.2	1102.6	1389.4	815.8	N
Wang et al., 2013 (34)	21	CA	20.5	110	52.2	1234.75	1654	815.5	Y
Wang et al., 2013 (34)	21	CA	20.5	110	44.5	1342.4	1869	815.8	Y
Wang et al., 2013 (34)	21	CA	20.5	110	37.2	1342.4	1869	815.8	Y
Wang et al., 2013 (34)	23	CA	37	105.9	37.2	1016.8	1389.4	644.2	N
Wang et al., 2013 (34)	24	CA	36.8	102.4	52.2	1102.6	1389.4	815.8	Y
Wang et al., 2013 (34)	24	CA	36.8	102.4	44.5	1096.5	1389.4	803.6	Y
Wang et al., 2013 (34)	24	CA	36.8	102.4	37.2	1130.6	1389.4	871.8	Y
Wang et al., 2013 (34)	25	CA	37.5	105.9	44.5	908	1031.3	784.7	N
Wang et al., 2013 (34)	25	CA	37.5	105.9	37.2	908	1031.3	784.7	N
Wang et al., 2013 (34)	26	CA	30.18	111.8	52.2	951.55	1031.3	871.8	N
Wang et al., 2013 (34)	26	CA	30.18	111.8	37.2	1191.2	1389.4	993	N
Wang et al., 2013 (34)	27	CA	36.6	110.3	37.2	1024.05	1389.4	658.7	N
Wang et al., 2013 (34)	28	CA	36.7	118.84	52.2	1130.6	1389.4	871.8	N
Wang et al., 2013 (34)	29	CA	32.5	90	44.5	1130.6	1389.4	871.8	N
Wang et al., 2013 (34)	29	CA	32.5	90	37.2	1130.6	1389.4	871.8	N
Wang et al., 2013 (34)	30	CA	29.66	91	37.2	1569.15	1654	1484.3	N
Wang et al., 2013 (34)	31	CA	39	76	52.2	1082.5	1389.4	775.6	Y
Wang et al., 2013 (34)	31	CA	39	76	44.5	1096.5	1389.4	803.6	Y
Wang et al., 2013 (34)	31	CA	39	76	37.2	1096.5	1389.4	803.6	Y
Wang et al., 2013 (34)	33	CA	30	121	44.5	1102.6	1389.4	815.8	N
Wang et al., 2013 (34)	34	CA	31.23	110.75	52.2	1130.6	1389.4	871.8	Y
Wang et al., 2013 (34)	34	CA	31.23	110.75	44.5	1191.2	1389.4	993	Y
Wang et al., 2013 (34)	34	CA	31.23	110.75	37.2	1191.2	1389.4	993	Y
Wang et al., 2013 (34)	35	CA	33.5	76	52.2	1102.6	1389.4	815.8	Y
Wang et al., 2013 (34)	35	CA	33.5	76	44.5	1082.5	1389.4	775.6	Y
Wang et al., 2013 (34)	35	CA	33.5	76	37.2	1191.2	1389.4	993	Y
Zhao et al., 2004 (*41*)	1	NLR	21.24	97.48	19.5	1235	1300	1170	N
Zhao et al., 2004 (*41*)	1	NLR	21.24	97.48	13.8	1235	1300	1170	N
Yang et al., 2007 (*42*)	15	ODA	28.5	111.5	16.1	1428.8	1691.2	1166.4	N
Yang et al., 2007 (*42*)	14	ODA	33	114.5	16.1	918.7	1109.1	728.3	N
Yang et al., 2007 (*42*)	13	ODA	30.5	109	16.1	1493.65	1880	1107.3	N
Yang et al., 2007 (*42*)	7	ODA	28.5	110.5	16.1	1565.85	1691.2	1440.5	N
Yang et al., 2007 (*42*)	5	ODA	29.5	114.5	16.1	1475.55	2074.4	876.7	N
Yang et al., 2007 (*42*)	4	ODA	28.5	111	16.1	1505.45	1691.2	1319.7	N
Liang et al., 2003* (*42*)	15	CA	28.5	111.5	16.1	1221.5	1280.7	1162.3	N
Liang et al., 2003* (*42*)	14	CA	33	114.5	16.1	1221.5	1280.7	1162.3	N
Liang et al., 2003* (*42*)	13	CA	30.5	109	16.1	1221.5	1280.7	1162.3	N
Liang et al., 2003* (*42*)	7	CA	28.5	110.5	16.1	1221.5	1280.7	1162.3	N

Liang et al., 2003* (*42*)	5	CA	29.5	114.5	16.1	1221.5	1280.7	1162.3	N
Liang et al., 2003* (*42*)	4	CA	28.5	111	16.1	1221.5	1280.7	1162.3	N
Liang et al., 2003* (*42*)	15	CA	28.5	111.5	16.1	1071	1146	996	N
Liang et al., 2003* (*42*)	14	CA	33	114.5	16.1	1121	1281	961	N
Liang et al., 2003* (*42*)	13	CA	30.5	109	16.1	1071	1146	996	N
Liang et al., 2003* (*42*)	7	CA	28.5	110.5	16.1	1071	1146	996	N
Liang et al., 2003* (*42*)	5	CA	29.5	114.5	16.1	1071	1146	996	N
Liang et al., 2003* (*42*)	4	CA	28.5	111	16.1	1053.5	1146	961	N
Horiuchi et al. 2012 (*62*)	Khorat	-	17.15	102.3	142	400	700	100	N
Xu et al., 2008 (*90*)	Luhe	CA	25.1	101.2	8.45	2019.2	2244.8	1793.6	N
Xing et al., 2012 (*91*)	Xianfeng	CA	25.25	102.5	8.45	1418.5	1631	1206	N
Jaques et al., 2011a (*92*)	Xiaolongtan	CA	23.4	103.1	8.45	1427	1639	1215	N
Jaques et al., 2011a (*92*)	Lincang	CA	23.5	100	8.45	1303.5	1394	1213	N
Jaques et al., 2011b (*92*)	Xiaolongtan	CLAMP	23.4	103.1	8.45	1964	2300	1628	N
Su et al., 2013 (*93*)	Longmen	CLAMP	25.3	99.3	2.2	1735.5	1953.2	1517.8	N
Xie et al., 2012 (*94*)	Tuantian	CLAMP	24.4	98.4	2.8	1625.7	1843.4	1408	N
Xia et al., 2009 (*95*)	Xiaolongtan	CLAMP	23.3	103.1	8.45	1964.8	2300.7	1628.9	N
Xia et al., 2009 (*95*)	Xiaolongtan	CA	23.3	103.1	8.45	1427	1639	1215	N
Yao et al., 2011 (96)	Lunpola	CA	32.3	90	19.5	1113	1521	705	N
Yao et al., 2011 (96)	Toupo	CA	26.5	116.19	19.5	1195	1207	1183	N
Yao et al., 2011 (96)	Fushan	CA	19.5	109.56	19.5	1352	1521	1183	Y
Yao et al., 2011 (96)	Leizhou	CA	21.45	110	19.5	1278	1521	1035	Y
Yao et al., 2011 (96)	Beibuwan	CA	20.3	108.3	19.5	1321	1520	1122	Y
Yao et al., 2011 (96)	Yinggehai	CA	18.31	108.42	19.5	1373	1563	1183	Y
Yao et al., 2011 (96)	Zhujiangkou	CA	22.25	113.45	19.5	1352	1521	1183	Y
Yao et al., 2011 (96)	Weizhou	CA	21.02	109.03	19.5	1151	1206	1096	N
Yao et al., 2011 (96)	Xianju	CA	28.51	120.43	13.8	1151	1206	1096	N
Yao et al., 2011 (96)	Ninghai	CA	29.12	121.26	13.8	1151	1206	1096	N
Yao et al., 2011 (96)	Toupo	CA	26.5	116.19	13.8	1151	1206	1096	N
Yao et al., 2011 (96)	Shihti	CA	25.03	121.3	13.8	1288	1597	979	N
Yao et al., 2011 (96)	Fushan	CA	19.5	109.56	13.8	1398	1613	1183	Y
Yao et al., 2011 (96)	Leizhou	CA	21.45	110	13.8	1352	1521	1183	Y
Yao et al., 2011 (96)	Beibuwan	CA	20.3	108.3	13.8	1352	1521	1183	Y
Yao et al., 2011 (96)	Yinggehai	CA	18.31	108.42	13.8	1380	1577	1183	Y
Yao et al., 2011 (96)	Zhujiangkou	CA	22.25	113.45	13.8	1398	1613	1183	Y
Yao et al., 2011 (96)	Namling a	CA	29.43	89	8.45	956	1207	705	N
Yao et al., 2011 (96)	Namling b	CA	29.43	89	8.45	1151	1206	1096	N
Yao et al., 2011 (96)	Namling c	CA	29.43	89	8.45	1113	1521	705	N
Yao et al., 2011 (96)	Markam 1	CA	29	98	8.45	1117	1355	879	N
Yao et al., 2011 (96)	Markam a	CA	29	98	8.45	956	1207	705	N
Yao et al., 2011 (96)	Lunpola	CA	32.3	90	8.45	1308	1520	1096	N
Yao et al., 2011 (96)	Xiaolongtan	CA	23.48	103.11	8.45	990	1019	961	N
Yao et al., 2011 (96)	Fushan	CA	19.5	109.56	8.45	1218	1613	823	Y
Yao et al., 2011 (96)	Leizhou	CA	21.45	110	8.45	1278	1521	1035	Y
Yao et al., 2011 (96)	zeibuwan	CA	20.3	108.3	8.45	1380	1577	1183	Y
Yao et al., 2011 (96)	Yinggehai	CA	18.31	108.42	8.45	1373	1563	1183	Y
Yao et al., 2011 (96)	Zhujiangkou	CA	22.25	113.45	8.45	1398	1613	1183	Y
Sun et al., 2002 (*97*)	Shanwang	CLAMP	36.54	119.2	13.8	2195	2600	1790	N
Sun et al., 2011 (*98*)	Tengchong	CA	25	98.3	4.45	1460.6	1695.5	1225.7	N
Xie et al., 2007** (98)	Tengchong	CA	25	98.3	4.45	1834.3	1834.3	1834.3	N
Sun et al., 2011 (98)	Longling	CA	24.6	98.5	4.45	1035.3	1254.8	815.8	N
Sun et al., 2011 (98)	Eryuan	CA	26	99.8	4.45	1084	1546.5	621.5	N
Sun et al., 2011 (98)	Tengchong	CA	25	98.3	2.2	1202.7	1546.5	858.9	N
Sun et al., 2011 (98)	Longling	CA	24.6	98.5	2.2	1235	1300	1170	N
Sun et al., 2011 (98)	Jianchuan	CA	26.4	98.6	2.2	1266.8	1546.4	987.2	N
Yao et al., 2009 (*99*)	Changchang	NLR	19.5	110.4	48.1	949	1113.3	784.7	N
Liang et al., 2003* (*89*)	Shanwang	CA	36	118	13.8	1221.5	1281	1162	N
Liu et al., 2011 (100)	1	CA	39	119	19.5	1127.5	1520	735	Y
Liu et al., 2011 (100)	2	CA	36.6	117.1	19.5	1127.5	1520	735	N
Liu et al., 2011 (100)	6	CA	40	94.4	19.5	1377	1632	1122	Y
Liu et al., 2011 (100)	4	CA	39.3	117.3	41.21	1164	1206	1122	Y
Liu et al., 2011 (100)	8	CA	36.2	102	19.5	1097.5	1298	897	Y
Liu et al., 2011 (100)	9	CA	34	108	18.2	1308	1520	1096	N
Liu et al., 2011 (100)	9	CA	34	108	18.2	1336.5	1577	1096	N
Liu et al., 2011 (100)	1	CA	39	119	13.8	1188	1724	652	Y
Liu et al., 2011 (100)	11	CA	33	118	13.8	1151	1206	1096	N
Liu et al., 2011 (100)	12	CA	36.6	119	13.8	1127.5	1520	735	N
Liu et al., 2011 (100)	13	CA	33.4	114.4	13.8	1164	1206	1122	N
Liu et al., 2011 (100)	6	CA	40	94.4	13.8	978.5	1335	622	Y
Liu et al., 2011 (100)	8	CA	36.2	102	13.8	946.5	1520	373	Y
Liu et al., 2011 (100)	16	CA	39.3	117.3	12.6	1168.5	1215	1122	Y
Liu et al., 2011 (100)	17	CA	36.3	118.2	12.6	1196.5	1206	1187	N
Liu et al., 2011 (100)	4	CA	39.3	117.3	8.45	1168.5	1215	1122	Y
Liu et al., 2011 (100)	1	CA	39	119	8.45	970.5	1206	735	Y
Liu et al., 2011 (100)	12	CA	36.6	119	8.45	1127.5	1520	735	N

Liu et al., 2011 (100)	6	CA	40	94.4	8.45	914	1206	622	Y
Liu et al., 2011 (100)	8	CA	36.2	102	8.45	1161	1741	581	Y
Kou et al., 2006 (*101*)	Yunan	CA	26	99.5	2.2	1052.1	1484.3	619.9	N
Hao et al., 2012 (102)	Lop Nur	CA	39.47	88.23	8.45	836.5	1031	642	Y
Hao et al., 2012 (102)	Lop Nur	CA	39.47	88.23	3.55	990.2	1329.5	650.95	Y
Hao et al., 2012 (102)	Lop Nur	CA	39.47	88.23	1.3	842.7	1031.4	654	Y
Hao et al., 2012 (*102*)	Lop Nur	CA	39.47	88.23	0.465	364.6	368.2	361	Y
Quan et al., 2011 (103)	Fushun	CA	41.8	123	60.2	1126	1355	897	Y
Quan et al., 2011 (103)	Fushun	CA	41.8	123	57.25	1126	1355	897	Y
Quan et al., 2011 (103)	Fushun	CA	41.8	123	52.2	789.5	1206	373	Y
Quan et al., 2011 (103)	Fushun	CA	41.8	123	52.2	1198.5	1362	1035	Y
Quan et al., 2011 (103)	Fushun	CA	41.8	123	52.2	1126	1355	897	Y
Quan et al., 2011 (103)	Fushun	CA	41.8	123	44.5	1201.5	1281	1122	Y
Quan et al., 2011 (103)	Fushun	CA	41.8	123	44.5	1048.5	1362	735	Y
Quan et al., 2011 (103)	Fushun	CA	41.8	123	44.5	1198.5	1362	1035	Y
Quan et al., 2011 (103)	Fushun	CA	41.8	123	44.5	1126	1355	897	Y
Quan et al., 2011 (103)	Fushun	CA	41.8	123	37.2	1126	1355	897	Y

* in Yang 2007; ** in Sun 2011

Table S2. Summary and comparison of proxy paleoaltimetry and model paleogeography. Model data is palaeo-rotated and Pre-Industrial model elevations at the grid-point level and regional (all grid points surrounding the local grid point) level. Proxy reconstruction method is as a follows: 1) δ13Cc, 2) δ18Oc, 3) T(Δ47), 4) δD, 5) CLAMP, 6) Mammalian fossils, 7) Fossil pollens, 8) Fossil leaves and 9) Clumped isotopes. Adapted from Liu, 2016.

								Palaeogeographic reconstructions		Pre-Industrial elevation	
Block	**Locality/Basin**	**Age(Ma)**	**Palaeoelevation (m)**	**Method**	**Source**	**Latitude**	**Longitude**	**Grid-point**	**3x3 grid**	**Grid-point**	**3x3 grid**
	Gyirong	>7	< 2900-3400	1	(*104*)	28.9	85.3	4858-4789	3300-4915	5352	651-5352
			6700 +/-700	2	(*105*)	28.9	85.3	4858-4789	3300-4915	5352	651-5352
			5850(+1400/-730)	2	(*106*)	28.9	85.3	4858-4789	3300-4915	5352	651-5352
	Thakkhola	~7	4500-6300	2	(*107*)	28.4	83.5	3716-4216	186-4873	651	145-5352
			5700(+1410/-730)	2	(*106*)	28.4	83.5	3716-4216	186-4873	651	145-5352
		~11	3800-5900	2	(*107*)	28.4	83.5	3300-3716	279-4932	651	145-5352
			6240(+1410/-870)	2	(*106*)	28.4	83.5	3300-3716	279-4932	651	145-5352
	Zhada	9	5400+/-500	3	(*108*)	31.5	79.8	2683	804-4788	4482	193-5232
Himalayas		~9	5600+/-300	2	(*109*)	31.5	79.8	2683	804-4788	4482	193-5232
		~4	4000+/-300	2	(*110*)	31.5	79.8	3946	922-4901	4482	193-5232
	Qomolangma	~17	5100-5400	4	(*111*)	28	86.9	4932	1120-4932	2481	141-5352
	Qiabulin	21-19	2315+/-887	5	(*112*)	29.34	85.51	4596	2175-4628	5352	651-5352
	Liuqu	~56	919+/-887	5	(*112*)	29.2	87.83	1283	408-3971	5352	651-5352
	Namling	~31	4100(+1154/-1640)	2	(*113*)	29.7	89.1	3307	2998-3700	4884	1591-5352
		15	5200(+1370/-605)	2	(*114*)	29.7	89.1	4805	3347-4834	4884	1591-5352
			5100(+1300/-1900)	4	(*113*)	29.7	89.1	4805	3347-4834	4884	1591-5352
			4689+/-895	5	(*115*)	29.7	89.1	4805	3347-4834	4884	1591-5352
			4638+/-847	5	(*115*)	29.7	89.1	4805	3347-4834	4884	1591-5352
			5400+/-728	5	(*116*)	29.7	89.1	4805	3347-4834	4884	1591-5352
		~15	5540+/-887	5	(*112*)	29.7	89.6	4805	3347-4834	4884	1591-5352
		~5	5509(+1390/-1993)	4	(*113*)	29.7	89.1	4666-4915	2547-4915	4884	1591-5352
	Kailash	~24	4700-6700	2	(*117*)	31.1	81.3	3294	2968-4405	4692	184-5352
	Linzhou	60-50	4500+/-450	2	(*118*)	30.2	91.1	3235	1671-4265	4884	1591-5352
	Nima	~26	4500-4700	2	(*119*)	31.9	87.9	4122	1329-4310	5119	4692-5352
	Lunpola	40-35	>4000	2	(*120*)	32.2	88.9	3116-3169	2071-4159	5079	4497-5352
			3600-4100	4	(*121*)	32.2	88.9	3116-3666	2071-4159	5079	4497-5352
Lhasa		23-16	4260(+475/-575)	2	(*120*)	32.2	88.9	3411-3528	2784-4668	5079	4497-5352
			4500-4900	4	(*121*)	32.2	88.9	3411-3528	3411-4629	5079	4497-5352
		18-16	~3000	6	(*122*)	32.2	88.9	3411	3411-4629	5079	4497-5352
		23	3000-3200	7	(*123*)	32.2	88.9	3527	2784-4668	5079	4497-5352
		26-23	2770+/-530	4	(*124*)	32.2	88.9	3527-4310	1907-5185	5079	4497-5352
	Tangrayum Co	46	2590(+730/-910)	2	(*125*)	31.6	86.5	3285	1141-4390	5119	4692-5352
***	Bangoin	156-98	3000-4000	-	(*126*)	32.26	89.8	521-3945	0-3781	5079	4497-5352
	Heihuling	50-28	5200+/-600	2	(*127*)	34.5	87.5	1907-4019	0-4390	5239	1734-5303
	Markam	~23-16	3837(+1108-1574)	2	(*128*)	29.85	98.3	4568-4867	2276-4948	4461	1591-5036
Qiangtang	Markam	~37	3837(+1108/-1574)	2	(*128*)	29.8	98.6	3916 3690	0-4676	4460	1591-5036
	Xiaolongtan***	12.7-10	1645(+525-747)	2	(*128*)	23.8	103.2	1461-1945	320-4297	1433	189-2907
	Jianchuan***	~23-16	2601(+802-1140)	2	(*128*)	26.3	99.9	2277-2851	1547-4948	2908	557-4460
	Liming	~37	2700+/-300	2	(*24*)	27	99.8	1848-2322	1162-3250	2908	557-4460
	Tuotuohe	52-30	<2000	2	(*129*)	34	92.5	3493-4019	1558-4462	4787	3051-5303
		55-35	~4000	2	(*25*)	34	92.5	2305-4019	140-4463	4787	3051-5303
Hoh Xil		55-35	2000-2600	4	(*121*)	34	92.5	2305-4019	140-4463	4787	3051-5303
		40-37	2000	7	(*130*)	34	92.5	3638	2479-4323	4787	3051-5303
	Wudaoliang	~23	4000-4200	4	(*121*)	35.8	94.3	4086	2055-4808	4787	3051-5303
		~19	1400-3000	8	(*131*)	35.8	94.3	4131	1886-4552	4787	3051-5303
	Jiaolai	100-89	1500-3600	9	(*132*)	36.96	120.85	1598	704-1716	0	0-635

Table S3. GCM sensitivity simulations for each geologic stage-specific simulation June–September (JJAS) data for the strength of the Hadley circulation (vertical velocities; Pa/s) over 21.75°N to 38.75°N and between 1000 and 200 hPa in EA. Walker circulation strength (vertical velocities; Pa/s) between 103.125°E - 114.375°E longitude and 1000hPa - 200hPa in East Asia. Negative values signify descending airmass. The mean temperature gradient slope (K/° of latitude) for 52.5°N-105°N between 30°N-90°N. Monsoon Precipitation Index (MPI) as defined by Wang, et al. 2008. The seasonal range in precipitation (mm/day^{-1}). Monsoonal (0 is not a monsoon regime, 1 is a monsoon regime) as defined by Wang, et al. 2008 where a MPI over >0.5 and a seasonal range greater than 2mm/yr^{-1} defines a monsoonal regime. The CO2 (ppm) concentration of each geologic stage simulation.

STAGE	Precipitation (mm/day)	Hadley circulation (Pa/s)	Walker circulation (Pa/s)	Temperature Gradient (K/° Lat)		Precipitation seasonal range		
NAME	JJAS	JJAS	JJAS	JJAS	MPI	(mm/day).	Monsoonal? 0=no, 1=yes	CO_2
Berriasian	3.44	-0.027	-0.058	-0.51	0.35	1.03	0	1120
Valanginian	6.03	-0.028	-0.060	-0.61	1.14	3.92	1	1120
Hauterivian	6.97	-0.026	-0.035	-0.59	1.33	4.63	1	1120
Berremian	6.44	-0.016	-0.025	-0.49	1.14	3.87	1	1120
Aptian	5.42	-0.017	-0.014	-0.49	1.41	3.73	1	1120
Albian	3.19	-0.005	-0.012	-0.45	1.06	1.80	0	1120
Cenomanian	1.28	-0.009	-0.016	-0.36	0.07	0.07	0	1120
Turonian	1.28	-0.006	-0.006	-0.40	0.12	0.13	0	1120
Coniacian	1.36	-0.009	-0.010	-0.43	0.18	0.19	0	1120
Santonian	1.48	-0.010	-0.009	-0.48	0.77	0.66	0	1120
Campanian	2.04	-0.014	-0.022	-0.47	1.07	1.21	0	1120
Maastrichtian	2.29	-0.015	-0.026	-0.42	1.30	1.60	0	1120
Danian	4.25	-0.023	-0.049	-0.46	1.16	2.77	1	1120
Selandian	4.08	-0.021	-0.042	-0.42	1.20	2.67	1	1120
Thanetian	6.20	-0.032	-0.077	-0.45	1.08	3.86	1	1120
Ypresian	5.91	-0.032	-0.058	-0.42	1.07	3.64	1	1120
Lutetian	6.11	-0.036	-0.067	-0.46	0.92	3.30	1	1120
Bartonian	7.29	-0.036	-0.049	-0.48	0.82	3.77	1	1120
Priabonian	7.52	-0.035	-0.047	-0.49	0.91	4.40	1	1120
Rupelian	7.65	-0.045	-0.055	-0.55	1.14	5.34	1	560
Chattian	6.97	-0.040	-0.065	-0.56	0.91	4.41	1	560
Aquitanian	6.30	-0.033	-0.064	-0.60	0.78	3.68	1	400
Burdigalian	6.46	-0.028	-0.076	-0.60	0.86	4.11	1	400
Langhian	6.68	-0.031	-0.067	-0.62	0.89	4.23	1	400
Serrevallian	8.01	-0.034	-0.060	-0.59	1.11	5.87	1	400
Tortonian	7.79	-0.032	-0.049	-0.62	0.84	4.98	1	400
Messinian	8.54	-0.033	-0.037	-0.63	1.02	5.72	1	400
Zanclean	8.94	-0.031	-0.041	-0.62	1.03	6.08	1	400
Piacenzian	8.96	-0.024	-0.033	-0.61	1.37	6.56	1	400
Gelasian	7.71	-0.022	-0.030	-0.61	1.37	5.68	1	280
Pre-Industrial	7.37	-0.029	-0.041	-0.67	1.29	5.76	1	280
Sensitivity experiments:								
Berriasian	3.19	-0.024	-0.052	-0.53	0.37	0.96	0	560
Hauterivian	6.34	-0.021	-0.024	-0.59	1.32	4.19	1	560
Aptian	5.65	-0.016	-0.022	-0.49	1.36	3.99	1	560
Cenomanian	1.22	-0.006	-0.013	-0.38	0.00	0.00	0	560
Santonian	1.24	-0.009	0.001	-0.48	0.45	0.39	0	560
Campanian	1.65	-0.011	-0.013	-0.47	0.56	0.63	0	560
Maastrichtian	1.92	-0.016	-0.024	-0.43	1.03	1.14	0	560
Ypresian	4.96	-0.026	-0.053	-0.42	0.94	2.83	1	560
Bartonian	6.78	-0.035	-0.056	-0.50	0.95	3.96	1	560
Rupelian	7.68	-0.036	-0.050	-0.55	0.95	4.95	1	1120
Chattian	7.50	-0.041	-0.068	-0.55	0.93	4.81	1	1120

Langhian	7.48	-0.032	-0.070	-0.64	0.98	5.14	1	560
Serrevallian	8.99	-0.026	-0.050	-0.63	1.21	6.93	1	560
Gelasian	8.64	-0.025	-0.028	-0.62	1.34	6.24	1	560

Table S4. Correlations between different processes during all geologic stages, Cretaceous stages, Paleogene stages, and Neogene stages. Correlations are calculated from values in table S3.

Correlation	Time period			
	All stages	Cretaceous	Paleogene	Negoene
Precipitation and Hadley circulation	-0.78	-0.72	-0.91	0.17
Precipitation and Walker circulation	-0.56	-0.53	-0.23	0.76
Hadley circulation and N.Hem latitudinal Temperature Gradient	0.54	0.84	0.79	-0.11
Hadley circulation and N.Hem latitudinal Temperature Gradient	0.40	0.70	0.15	-0.44

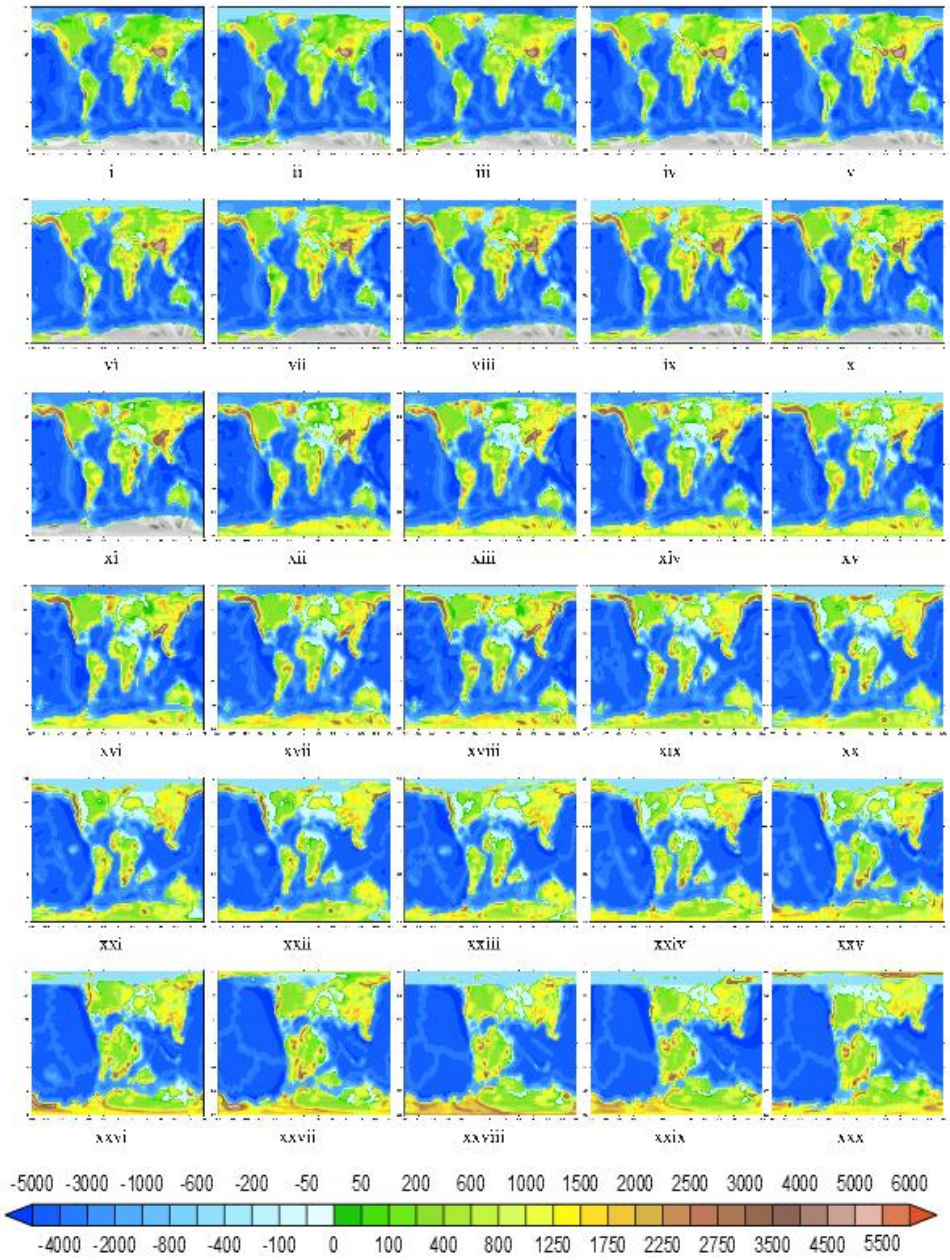

Fig. S1. Orography and bathymetry in (i) Gel, (ii) Pia, (iii) Zan, (iv) Mes, (v) Tor, (vi) Ser, (vii) Lan, (viii) Bur, (ix) Aqu, (x) Cha, (xi) Rup, (xii) Pri, (xiii) Bar, (xiv) Lut, (xv) Ypr, (xvi) Tha, (xvii) Sel, (xviii) Dan, (xix) Maa, (xx) Cmp, (xxi) San, (xxii) Con, (xxiii) Tur, (xxiv) Cen, (xxv) Alb, (xxvi) Apt, (xxvii) Brm, (xxviii) Hau, (xxix) Val, (xxx) Ber geologic stage simulations.

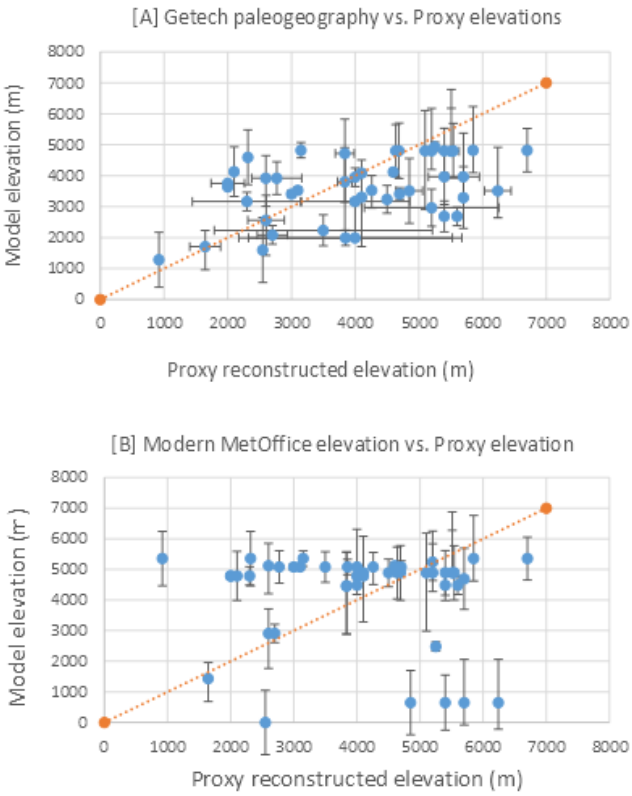

Fig. S2. EA proxy paleoaltimetry data versus prescribed paleogeography. Median proxy elevation data (Table S2) over the last 150 Myr compared to model paleogeography representative stage closest to the proxy age [A] and Pre-Industrial model elevation [B]. Vertical error bars represent uncertainty range in the proxy reconstructed height (m). Horizontal bars represent age uncertainty in the proxy and associated range in model elevations over that specified age boundaries.

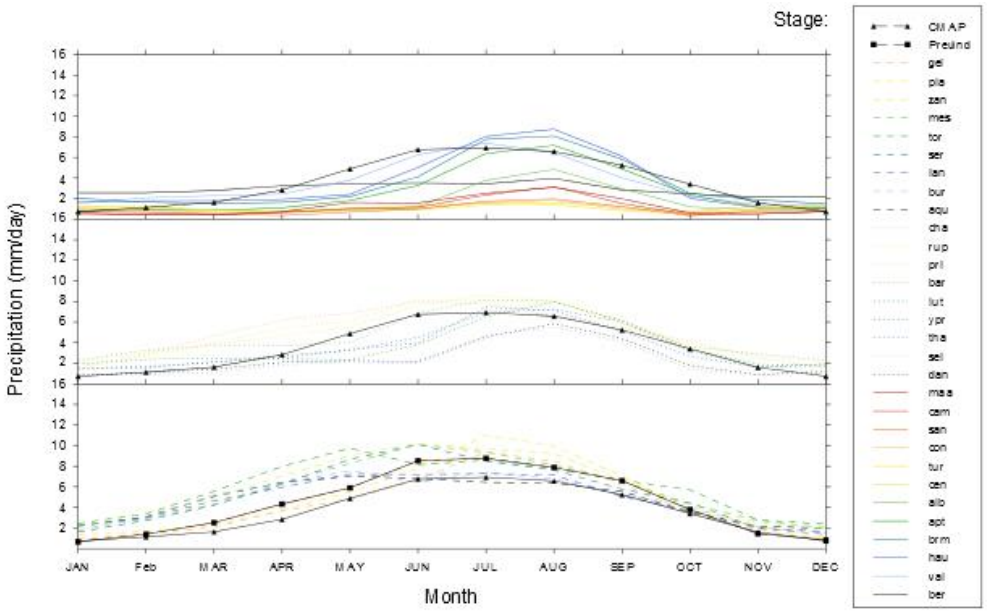

Fig. S3. Precipitation seasonality. Seasonal distribution of precipitation for each geologic stage during the Cretaceous (top panel), Paleogene (middle panel) and the Neogene (bottom panel) in the EAM region. CMAP observations (1979-2011) are included for comparison.

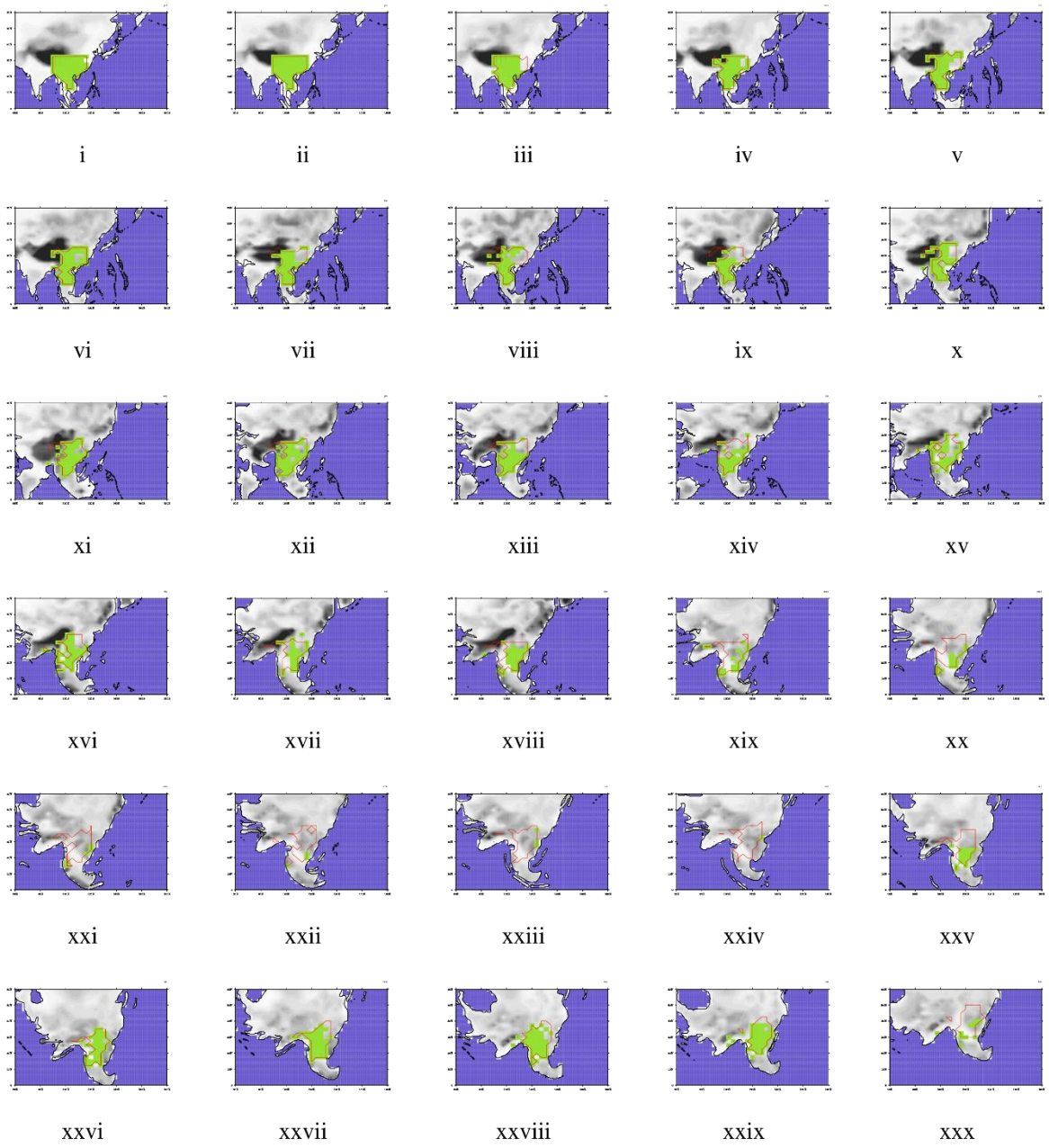

Fig. S4. Monsoonal regions in (i) Gel, (ii) Pia, (iii) Zan, (iv) Mes, (v) Tor, (vi) Ser, (vii) Lan, (viii) Bur, (ix) Aqu, (x) Cha, (xi) Rup, (xii) Pri, (xiii) Bar, (xiv) Lut, (xv) Ypr (xvi) Tha, (xvii) Sel, (xviii) Dan, (xix) Maa, (xx) Cmp, (xxi) San, (xxii) Con, (xxiii) Tur, (xxiv) Cen, (xxv) Alb, (xxvi) Apt, (xxvii) Brm, (xxviii) Hau, (xxix) Val, (xxx) Ber simulations. Terrestrial monsoonal regions (Green) for each geologic stage in East Asia within the pre-defined paleo-rotated monsoon region (red outline).

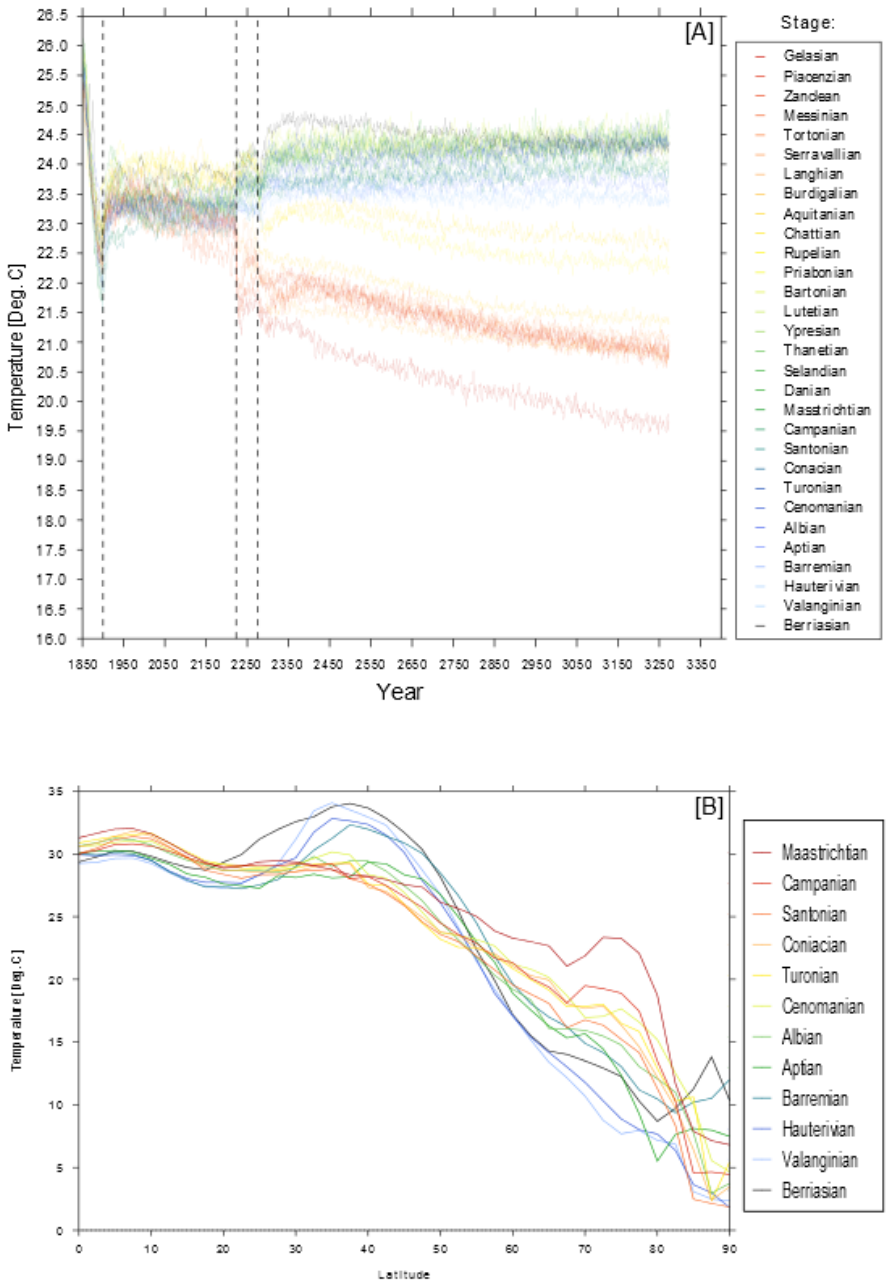

Fig. S5. Simulation spin-up of SST and zonal 1.5-m air temperature (°C). [A] Model SST spin-up for each geologic stage from the beginning of the Cretaceous (~150 Ma ago) to the end of the Pliocene (~2.2 Myr), further discussion on model setup and methodology can be found in Lunt et al. (2016). Northern hemisphere pole-equator zonal mean summer (JJAS) 1.5 m air temperature for the Cretaceous simulations.

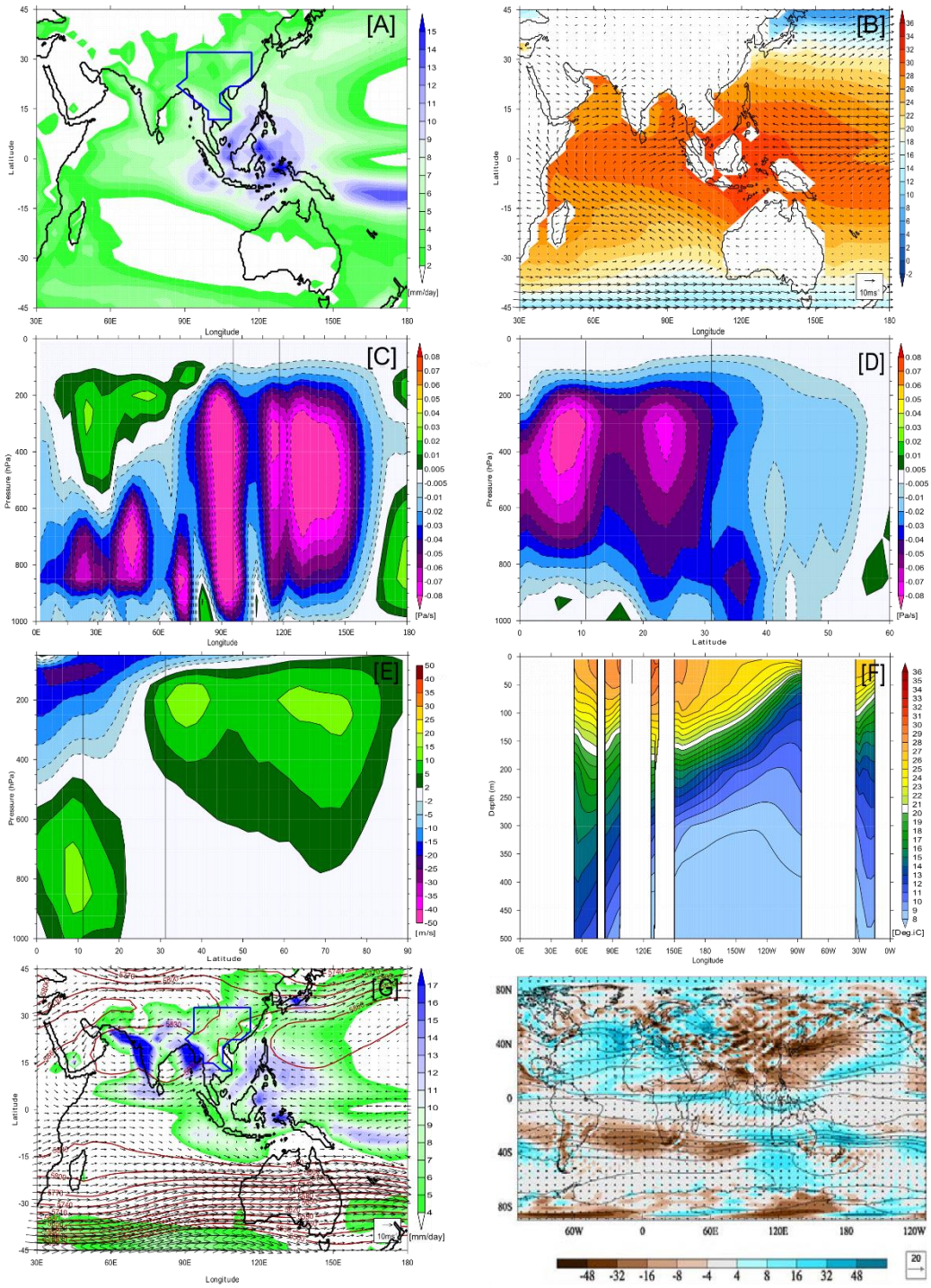

Fig. S6. Preindustrial mean fields. [A] Pre-industrial mean annual precipitation and [B] sea surface temperatures. The EAM is overlaid (blue outline). [C] Wettest month meridional (17.5°N-22.5°N), [D] zonal (105°E-112.5°E) vertical velocity cross-sections over East Asia, negative values indicate vertical ascent, positive values indicate vertical descent. [E] wettest month u-wind zonal cross-section (105°E-112.5°E) over East Asia, negative values indicate

easterlies and positive values indicate westerlies. Vertical black lines depict maximum and minimum latitudinal and longitudinal extent of the East Asian region. [F] Mean annual meridional (10°S-10°N) depth integrated ocean temperature (°C). [G] 500mb geopotential height (isolines). [H] Rossby waves sources in JJA, the colors indicate the Rossby wave source, the contours show the absolute vorticity, and the vectors show the divergent component of the flow all at 150mb (centered on the HTR).

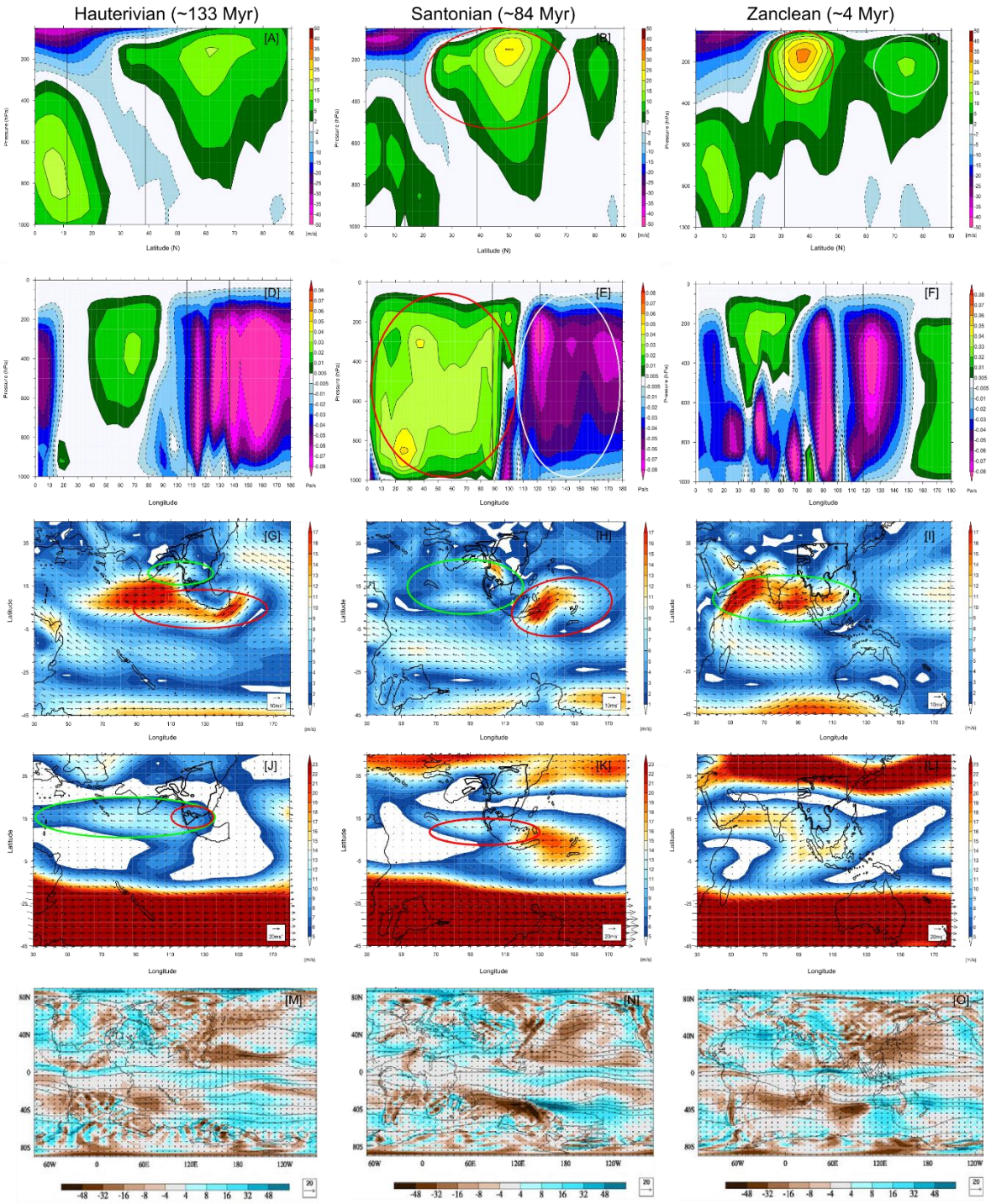

Fig. S7. Wind profiles and vertical velocities in the Hauterivian, Santonian, and Zanclean. Wettest month meridional mean (105°N-112.5°N) U-wind speed (m/s) cross-sections over East Asia for the Hauterivian [A], Santonian [B] and Zanclean [C]. Negative values indicate easterlies, positive values show westerlies. Zonal mean (17.5°E-22.5°E) vertical velocity (Pa/s) cross-sections over East Asia for the Hauterivian [D], Santonian [E]

and Zanclean [F]. Negative values indicate vertical ascent while positive values indicate vertical descent. Vertical black lines depict maximum and minimum latitudinal and longitudinal extent of the EAM region. 850mb wind strength (m/s) and direction for the Hauterivian [G], Santonian [H] and Zanclean [I] depicting the strength and position of the Somali Jet. 200mb wind strength (m/s) and direction for the Hauterivian [J], Santonian [K] and Zanclean [I] depicting the strength and position of the Tropical Easterly Jet. Red and green circles indicate regions of interest highlighted in the main text. Rossby waves sources in JJA for [M] Hauterivian, [N] Santonian and [O] Zanclean. The colors shows the Rossby wave source, the contours show the absolute vorticity, and the vectors show the divergent component of the flow all at 150 mb (centered on the HTR).

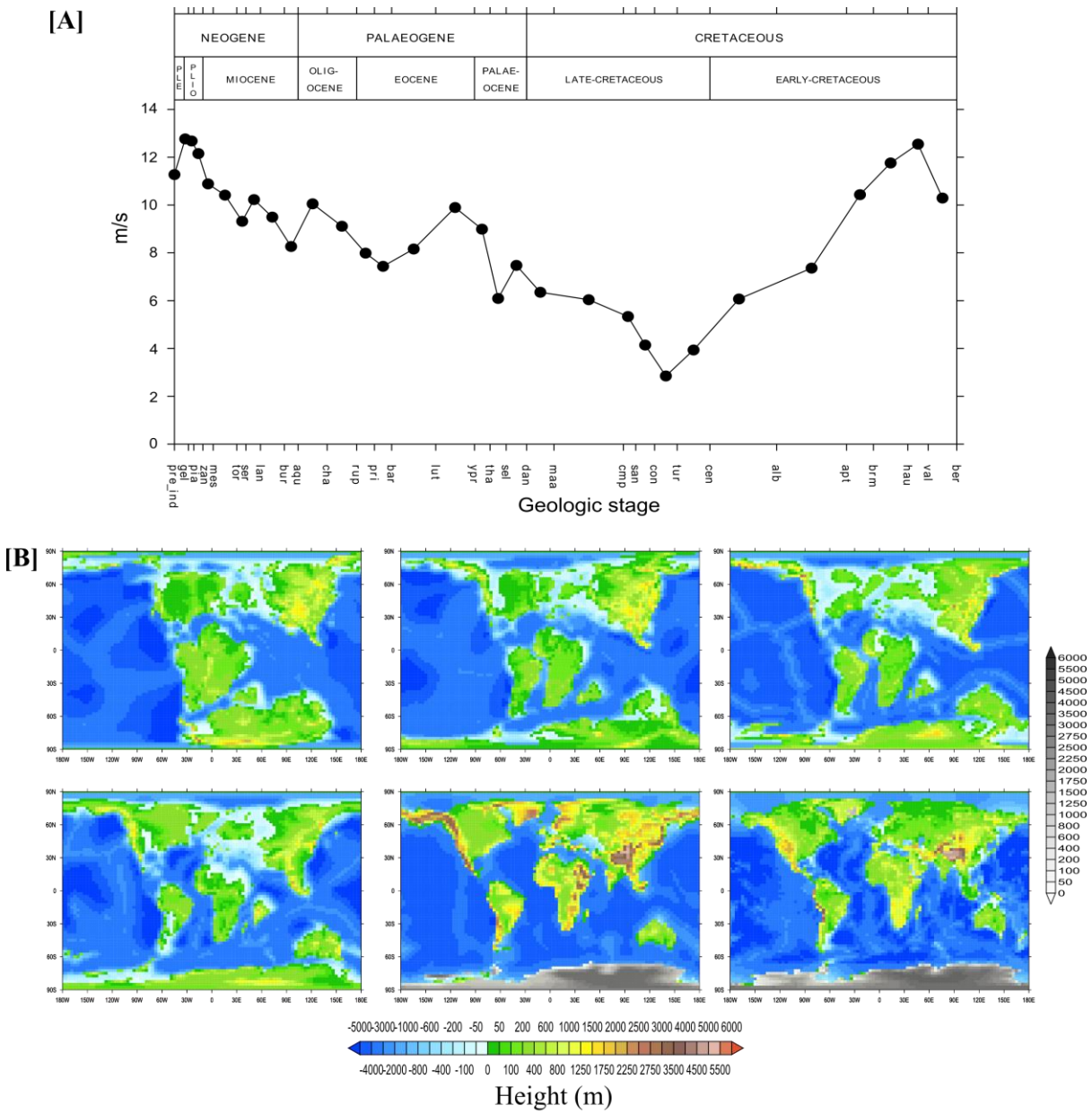

Fig. S8. Mean SLLJ strength and alternative paleogeographies. [A] Mean (0°N-25°N, 70°E-90°E) 850 mb zonal wind strength (m/s) timeseries during the wettest month for each geologic stage. [B] Alternative paleogeographies indicated in Figure 1b depicting the bathymetry and topography (m). Valanginian (top left), Albian (top middle), Turonian (top right), Maastrichtian (bottom left), Chattian (bottom middle) and Paicenzian (bottom right).